Dielectrophoresis-assisted plasmonic trapping of dielectric nanoparticles

Mohammad Asif Zaman,* Punnag Padhy, Paul C. Hansen, and Lambertus Hesselink
Department of Electrical Engineering, Stanford University Stanford, California 94305, USA
(Received 24 January 2017; published 27 February 2017; corrected 8 May 2017)

A method for efficiently trapping nanoparticles using a dielectrophoresis (DEP)-assisted plasmonic trap is presented. The proposed method overcomes the range limitations of a conventional plasmonic trap by employing a long-range DEP force to draw a nanoparticle closer to the plasmonic trap. To create the plasmonic trap, a C-shaped engraving is used as it can trap a nanoparticle in a very small volume near the surface. A nanopillar is selected as the electrode to generated the DEP force as its height allows the force to extend further away from the surface. Extensive numerical simulations are performed to evaluate the performance improvement of the proposed scheme over conventional plasmonic trapping methods. The simulations show that the proposed scheme increases the probability of a successful trapping event by a factor of approximately three.

DOI: 10.1103/PhysRevA.95.023840

I. INTRODUCTION

Noninvasive trapping and manipulation of submicron-sized particles is an important area of research in the field of nanotechnology and bioscience [1–3]. Optical tweezers [4,5] employing focused laser beams have been successfully used to trap and manipulate small particles and biological samples [6,7]. However, the diffraction limit sets a bound on the maximum resolution that can be achieved using a single focused laser beam. Near field optical trapping techniques such as plasmonic traps have been developed to overcome the focusing limitations of conventional optical tweezers [8,9]. When a plasmonic structure is illuminated, it can confine light tighter than the diffraction limit, making it possible to trap subwavelength sized objects. The evanescent fields created near the surface of a metallic structure generates an optical gradient force which can be used to trap a nanoparticle. Compared to the three-dimensional approach of conventional optical tweezers, the surface characteristics of plasmonic traps make it possible to design a 2D array of such traps [10–14]. The potential of such parallelization makes plasmonic traps an attractive choice for laboratory-on-a-chip applications.

In plasmonic trapping experiments, a liquid medium containing the particles to be trapped is placed on top of the plasmonic structure. A laser is used to illuminate the structure from the top or bottom side. If the incident light is near the plasmon resonance wavelength, a very high near-field intensity is achieved in the vicinity of the metal structure. The plasmon resonance wavelength and the corresponding intensity enhancement depends on the geometry of the structure and the optical properties of the metal and the surrounding dielectric. Unlike the far-field focusing used in optical tweezers, the near-field of the plasmonic structure is confined to subwavelength dimensions. The high-intensity gradient in the near-field creates a strong optical force [15] that can trap particles smaller than the exciting wavelength. Several plasmonic structures have been developed, such as circular apertures [16], nanopillars [17–19], bowtie antenna [20], and C-shaped apertures and engravings [10,11]. These structures have been successfully used in many applications.

The characteristics that make plasmonic traps desirable can also lead to some unwanted issues. As plasmonic traps operate in the evanescent field region, which decreases exponentially with the distance from the resonant surface, the associated optical forces are substantial only in a very small region. Although the resulting trap has subwavelength resolution, its effective range is severely limited. Unlike optical-tweezers, plasmonic traps cannot be moved freely in 3D space to pluck particles from the liquid medium. In most cases, a focused laser beam is used to manually drag a particle near the plasmonic trap to load it. This *loading* problem can be a serious issue. Without manual loading, it may take a very long time to successfully trap a particle if the particle density in the medium is low. The loading problem can be a bottleneck in implementing large-scale parallelization of such traps for laboratory-on-a-chip applications. In this paper, we propose the use of the dielectrophoresis (DEP) force to draw particles near the plasmonic trap for more efficient particle loading.

The DEP force is the time averaged net force a dielectric particle experiences when it is submerged in a nonuniform AC electric field. Like the optical force, the DEP force originates from the gradient of the electric field intensity. It is created by applying an AC voltage (with frequencies usually ranging from kHz to MHz) across a pair of electrodes. The resulting electric field distribution depends on the shape of the electrodes. The magnitude of the force depends on the gradient of the field intensity, dielectric constants of the particle and the surrounding medium, the frequency of the excitation, and the size of the particle. DEP has been successfully used to trap and manipulate small particles for various applications [21–24]. Unlike near-field optical forces, DEP forces extend much farther away from the electrodes resulting in longer range. However, the DEP traps do not confine fields as tightly as the plasmonic traps. As a result, the position distribution of a particle in a DEP trap spans a much larger volume than that of a particle trapped in a plasmonic trap. The difference in resolution becomes more prominent as the particle size goes down. This inferior resolution makes the DEP trap less-suitable for applications demanding higher precision.

A trapping scheme capable of exerting long-range force as well as maintaining a high resolution is highly desirable. In this work, we propose a composite trapping method that uses both DEP and optical forces. We posit that using the DEP

*zaman@stanford.edu

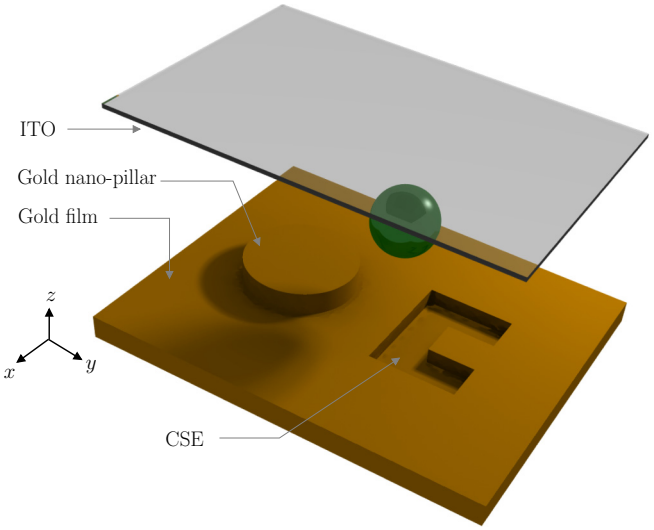

FIG. 1. Three-dimensional representation of the proposed DEP-assisted plasmonic trap. The green sphere represent a nanoparticle.

force in conjecture with the optical force can help solve the loading problem of plasmonic traps. The proposed scheme consists of a DEP trap in close proximity to a plasmonic trap. The separation between them is small enough so that there is overlapping between the trapping regions of the two traps. In such a system, if the long-range DEP trap is activated first (with the plasmonic trap turned off), a particle will be drawn toward the trapping region. After a certain time, if the DEP force is turned off and the optical force is turned on, a particle near the DEP trap will be transferred to the nearby plasmonic trap. This scheme combines the long-range capabilities of the DEP force with the high-resolution characteristics of the plasmonic trap. To the best of the authors' knowledge, no simulation or experimental work on such a scheme has been reported in the literature to date.

Appropriate structures must be selected to implement the proposed scheme. For the plasmonic trap, we select a structure that can produce high trapping resolution. The C-shaped structures (apertures or engravings) can achieve a resolution of less than $\lambda/10$ and create strong near-field enhancement [25,26]. Due to the asymmetry of the C-shape, the generated field enhancement is polarization dependent, which can be useful when trying to excite a single trap in a multitrap system [10]. Based on these desirable properties, we use a gold C-shaped engraving (CSE) [11,12] as the plasmonic trap in this paper. To generate the DEP force, a nanopillar is used as one of the electrodes. An indium tin oxide (ITO) plate is selected as the other electrode. The nanopillar electrode has several advantages that make it suitable for the proposed scheme. The height of the nanopillar allows it to exert DEP force farther away from the surface, which helps to increase the trapping range. Furthermore, the height of the nanopillar can be fine-tuned to control the overlap between the trapping regions of the DEP trap and the plasmonic trap. An optimum overlap is required so that a particle trapped near the nanopillar can be transferred to the CSE with high reliability. For these reasons, we use a nanopillar-CSE structure to test the proposed trapping scheme.

A comprehensive numerical analysis is performed to quantify the effectiveness of the proposed scheme. A full wave analysis is performed to calculate the fields. Forces are calculated using Maxwell's stress tensor. A Brownian dynamics model incorporating hydrodynamic interactions and a reflection mechanism is used to model the particle motion. The motion of a single nanoparticle is simulated a large number of times to obtain a statistical distribution of particle position. Using these statistics, the performance of the proposed DEP-assisted plasmonic trapping scheme is compared with that of a stand-alone plasmonic trapping case. It is found that the proposed scheme shows a significant increase in particle trapping probability.

II. GEOMETRY AND TRAPPING SCHEME

The geometry of the proposed structure is shown in Fig. 1. A schematic of top view and cross-sectional view are shown in Fig. 2. The geometry consists of a CSE on a gold base, a gold nanopillar, and an ITO plate. The radius and the height of the nanopillar are denoted by r_{np} and h_{np}, respectively. The top surface of the nanopillar is taken to be a smooth curved ellipsoid to represent realistic geometry obtained from nanofabrication. The xy plane dimensions of the CSE are defined by a single parameter, α. This particular geometry of C structures provide maximum intensity enhancement and

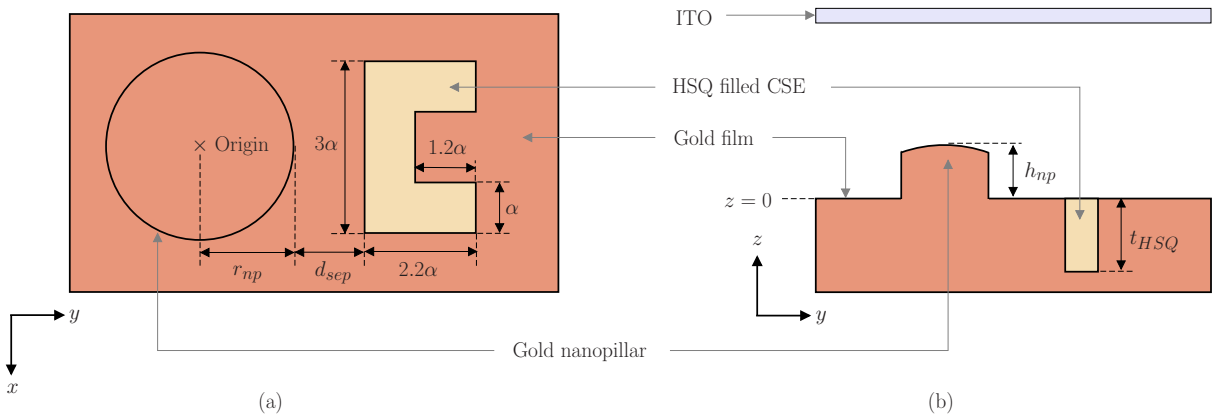

FIG. 2. Two-dimensional views of the proposed geometry. (a) Top view (xy plane). (b) Cross-sectional view ($x = 0$).

TABLE I. Geometric parameters.

Parameter	Size (nm)
CSE characteristic parameter, α	60
Nanopillar height, h_{np}	120
Nanopillar radius, r_{np}	150
Separation between CSE and nanopillar, d_{sep}	150
Depth of the engraving, t_{HSQ}	150
Polystyrene particle radius, r_o	150

has been successfully used for trapping applications [11,25]. The CSE is filled with the dielectric hydrogen silsesquioxane (HSQ) [11]. A polystyrene sphere of radius 150 nm is selected as the nanoparticle. As polystyrene spheres are chemically very inert and proteins and ligands can easily attach onto their surface, they have been widely used in biomedical research [27,28]. Due to these reasons, a polystyrene sphere is an appropriate choice for the current study.

The numerical values of the geometric parameters used for the simulation are shown in Table I. The centers of the nanopillar and the CSE in xy plane are located at (0,0) and $(0, r_{np} + d_{sep} + 1.1\alpha) = (0, 366\,\text{nm})$ points, respectively. The base of the nanopillar and the top of the CSE are located at $z = 0$ plane. A water medium containing a polystyrene nanoparticle is sandwiched between the gold and the ITO plate. The ITO and the nanopillar act as the two electrodes for the DEP system. An AC voltage applied between the gold base and the ITO generates the DEP force. Such nanopillar-shaped electrodes have been successfully used for DEP trapping [24]. Light from a laser is considered to be applied from the top (through the transparent ITO) to excite the CSE. This type of excitation configuration has been successfully used for trapping applications [11,12].

To use this geometry for efficient particle trapping, the AC voltage is applied first to draw the nanoparticle near the nanopillar due to DEP. After a given time, the AC voltage is turned off and the laser is turned on. Since the particle is likely to be already close to the nanopillar (and hence close to the CSE), the optical force from the CSE can trap it more easily. The term *hand-off* is used in this paper to refer to the transfer of a particle from the nanopillar to the CSE.

The orientation of the CSE and its placement relative to the nanopillar can affect the probability of a successful hand-off. Here, the separation between the CSE and the nanopillar is taken to be $d_{sep} = 150$ nm, which is a realistic value that can be achieved by nanofabrication. The geometric parameter values are selected based on simulations of multiple geometric configurations. The CSE is excited when the polarization of incident light is parallel to the arms of the C, which is along the y axis in Fig. 2. Although the nanopillar is used mainly as an electrode for DEP, it also exhibits a plasmonic resonance. Two high-field-intensity lobes are formed on the top surface of the nanopillar. The lobes are oriented parallel to the polarization axis of the incident light [17,18]. For the coordinate system shown in Fig. 2, the nanopillar will focus light near $(0, \pm r_{np}, h_{np})$ points for a y polarized incident light. So, when the optical excitation is turned on, the particles located near the nanopillar will be moved toward these points. As the point $(0, r_{np}, h_{np})$ is close to the CSE, a nanoparticle located near that can easily be transferred toward the CSE. Since the optical force from the CSE is much stronger than that from the nanopillar (≈10 times stronger), there is a very small probability (<0.1%) of the reverse hand-off situation (particle transfer from CSE to nanopillar). The probability of a successful hand-off between the nanopillar and the CSE depends on the distance between the focus regions of the two structures. Placing the two structures along the polarization axis of the light (with proper orientation of the CSE) minimizes the distance a nanoparticle must travel for hand-off and thus increase the probability of a successful trapping event.

III. DEP FORCE CALCULATION

The time-averaged DEP force acting on a spherical particle with radius r_o surrounded by a medium with complex dielectric function (relative permittivity) $\tilde{\epsilon}_m$ can be approximated as [29,30]

$$\langle \mathbf{F_{DEP}} \rangle = 2\pi r_o^3 \epsilon_0 \mathrm{Re}[\epsilon_m(\omega)\tilde{C}_M(\omega)\nabla(|\mathbf{E}|^2)]. \quad (1)$$

Here, $|\mathbf{E}|$ and ω are the amplitude and frequency of the electric field, respectively, ϵ_0 is the permittivity of free space, and $\tilde{C}_M$ is the Clausius-Mossotti factor given by

$$\tilde{C}_M(\omega) = \frac{\tilde{\epsilon}_p(\omega) - \tilde{\epsilon}_m(\omega)}{\tilde{\epsilon}_p(\omega) + 2\tilde{\epsilon}_m(\omega)}. \quad (2)$$

Here, $\tilde{\epsilon}_p$ is the complex dielectric function of the nanoparticle material (polystyrene). The complex dielectric functions take into account the absorption loss due to finite conductivity of the materials. They are modeled as [29]

$$\tilde{\epsilon}_{m,p}(\omega) = \epsilon_{m,p} - i\frac{\sigma_{m,p}}{\omega\epsilon_0}, \quad (3)$$

where $\epsilon_{m,p}$ are the real parts of the dielectric function and $\sigma_{m,p}$ are the conductivities. When the $\mathrm{Re}[\tilde{C}_M(\omega)] > 0$, the DEP force pushes the particle toward high-field-intensity regions. This is known as *positive DEP*. For $\mathrm{Re}[\tilde{C}_M(\omega)] < 0$, the opposite condition occurs and it is called *negative DEP*. The required frequency of the applied electric field for positive and negative DEP can be obtained by plotting the Clausius-Mossotti factor as a function of frequency [21].

Although Eq. (1) gives a good approximation of the DEP force, the dipole approximation that it is based on does not hold for high field gradients that are produced by very small electrodes (like a nanopillar) [31]. In this paper, we use Maxwell's stress tensor to calculate the force, which is a much more accurate method [32]. A commercial full wave Maxwell's equations solver (Comsol Multiphysics) is used to calculate the electric field distribution. The material properties used for the simulation are shown in Table II [10,21]. The

TABLE II. Material parameters.

Parameter	Material		
	Water	Polystyrene	HSQ
AC dielectric constant, ϵ_r	78.5	2.55	2.9
Conductivity, σ (S/m)	1×10^{-4}	1×10^{-2}	1×10^{-4}
Optical refractive index, n	1.33	1.58	1.4

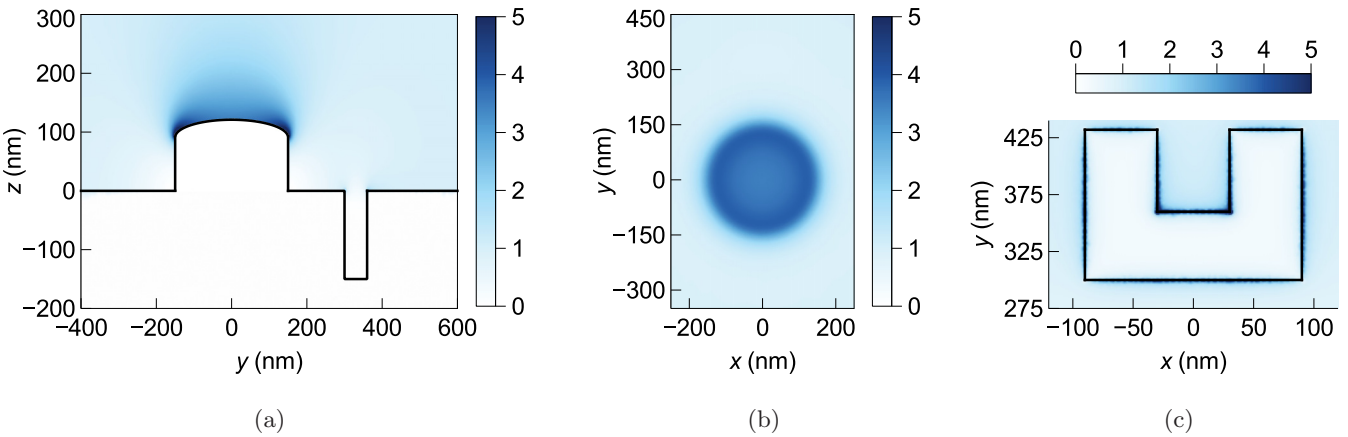

FIG. 3. AC field intensity enhancement, $|\mathbf{E}|^2/|\mathbf{E_0}|^2$ at 10 kHz (with no nanoparticle in the system). (a) yz cross-section at $x = 0$. (b) xy cross-section at $z = h_{\rm np}$. (c) xy cross-section at $z = 0$.

conductivity value used for the polystyrene nanoparticle takes into account the surface charge effects [21]. The simulation is performed at 10-kHz frequency. A background electric field of $|\mathbf{E_0}| = 0.18\,\mathrm{V}/\mu\mathrm{m}$ is applied between the ITO plate and the gold film. The resulting field-intensity enhancement, $|\mathbf{E}|^2/|\mathbf{E_0}|^2$, with no nanoparticle in the system, is shown in Fig. 3. The figures show that the high-field-intensity regions are located near the nanopillar top surface and extend outward. On the other hand, AC field intensity enhancement due to the CSE is limited to its top surface only. This is not surprising as the AC fields are expected to be affected by a pillar-shaped electrode and not by a planar dielectric-filled engraving.

At 10 kHz, $\mathrm{Re}[\tilde{C}_M(\omega)] > 0$, which leads to positive DEP forces. To calculate the force at a specific position of the nanoparticle, the electric field distribution with the nanoparticle in the system is calculated. Then Maxwell's stress tensor is integrated on the surface of the nanoparticle to calculate the force. To get the entire force-field, these calculations are repeated for each possible particle locations. The force profile obtained by varying the x position of the nanoparticle at $y = 0, z = 290$ nm (nanoparticle surface 20 nm above the top of the nanopillar) is shown in Fig. 4. The coordinates (x, y, z) indicate the position of the center of the spherical nanoparticle. It is noted that positive F_x exists for particle position left of the nanopillar axis which pushes the particle to the right. For particle position right of the nanopillar axis, the negative F_x pushes it toward the center again. The negative F_z values indicate the the particle is pulled down toward the nanopillar top surface. Due to symmetry of the nanopillar geometry, $F_y \approx 0$ at $y = 0$. The force values indicate a strong DEP trap centered around the top surface of the nanopillar. The potential energy along the x direction, U_x, is also shown in Fig. 4. It is defined as

$$U_x(x) = -\int_{-\infty}^{x} F_x(x')dx'. \tag{4}$$

The potential energy is normalized in k_BT units, where $k_B = 1.38 \times 10^{-23}\,\mathrm{J/K}$ is the Boltzmann constant and $T = 300\,\mathrm{K}$ is the temperature. It is observed that U_x is over $30k_BT$ deep. By sweeping the particle position along the y direction, a similar trend can be found for U_y. Since the thermal energy of the nanoparticle is on the order of a few k_BT, it can be concluded that the nanopillar produces a very strong trapping potential.

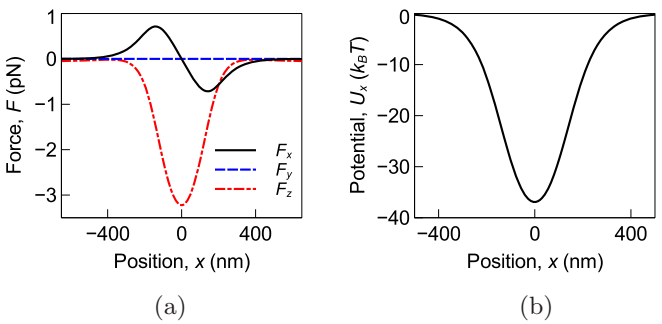

FIG. 4. DEP force and potential energy distribution for a 150-nm nanoparticle ($y = 0, z = 290$ nm). (a) DEP force components along x, y, and z directions. (b) DEP potential energy along x direction.

IV. OPTICAL FORCE CALCULATION

Optical forces are created by the gradient of the optical electric field intensity. At plasmonic resonance, a very high field intensity is formed near plasmonic structures. The intensity enhancements as a function of wavelength at 10 nm above the center of the CSE and at 10 nm above the top surface of the nanopillar are shown in Fig. 5. Light is assumed to be incident from the top (through the ITO plate) at an intensity of $1\,\mathrm{mW}/\mu\mathrm{m}^2$. It is observed that the intensity enhancement near the CSE is much larger. So, the optical force associated with the CSE will be much stronger than that of the nanopillar.

The wavelength at which plasmon resonance occur depends on the material properties of the metal and surrounding dielectric as well as the geometry of the structure. The refractive indices of the dielectric materials are listed in Table II. For calculating the spectral response shown in Fig. 5, a Drude model of the gold dielectric function is used [33]. The model fits experimental data points [34] and gives accurate results for wavelengths above 500 nm [35]. The wavelength of the illuminating light is selected to be 1064 nm, which is close

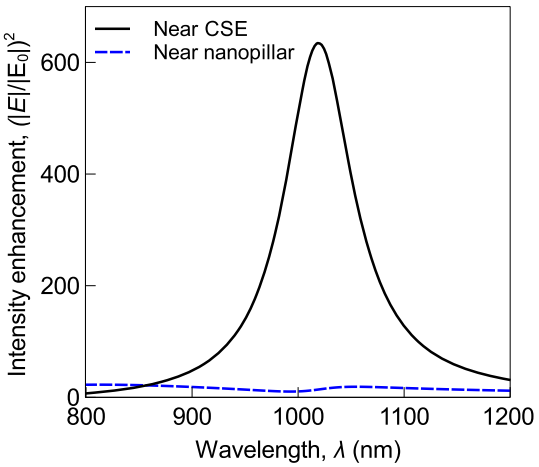

FIG. 5. Optical intensity enhancement near the CSE at $(0, -366\,\text{nm}, 10\,\text{nm})$ point and near the nanopillar at $(0, -150\,\text{nm}, 130\,\text{nm})$ point for light polarized along the y direction.

to the plasmon resonance wavelength of the CSE. The optical intensity distribution at this wavelength with no nanoparticle is shown in Fig. 6. It can be seen that significant field intensity enhancement occurs near the CSE. Some intensity enhancement also occurs near the nanopillar. To calculate the optical force-field, the fields are recalculated and the surface integral of the stress tensor is performed for each possible position of the nanoparticle. The force profile and the potential profile for a 1D position sweep are shown in Fig. 7. The values are measured at $y = 366\,\text{nm}$ and $z = 170\,\text{nm}$ (along the center of the CSE with the bottom surface of the nanoparticle located 20 nm above the gold surface). Compared to DEP, the optical force produces a narrower potential well, implying a tighter trap. However, the intensity distribution shows the smaller range of the near-field optical forces. To compare the range of the forces, the nanoparticle position is swept in the z direction along the center line of each structure. The separation is measured from the top of the structure (CSE or nanopillar) to the bottom surface of the nanoparticle. Due to symmetry, $F_x \approx 0, F_y \approx 0, F \approx F_z$. The coordinate-adjusted results are

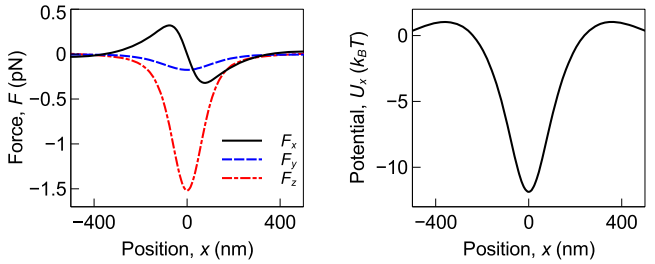

(a) (b)

FIG. 7. Optical force and energy distribution for a 150-nm particle ($y = 366\,\text{nm}$, $z = 170\,\text{nm}$). (a) Optical force components along x, y, and z directions. (b) Optical potential energy along x direction.

shown in Fig. 8. The higher slope of the optical force curve indicates its shorter range.

V. BROWNIAN DYNAMICS

Nanoparticles in a fluid medium exhibit Brownian motion due to thermal fluctuations. The motion of a nanoparticle immersed in a force-field (optical or DEP) can be accurately modeled using the modified Langevin equation [36,37]:

$$\dot{\mathbf{r}}(t) = \frac{1}{\gamma}\mathbf{F}(\mathbf{r},t) + \sqrt{\frac{2k_BT}{\gamma}}\mathbf{W}(t). \tag{5}$$

Here $\mathbf{r}(t)$ is the particle position at time t, γ is the viscous drag coefficient, $\mathbf{F}(\mathbf{r},t)$ is the force (optical and/or DEP) on the particle, and $\mathbf{W}(t)$ is a noise term that models random collisions with the fluid molecules. This stochastic differential equation can be numerically solved using the Euler-Maruyama method [38]:

$$\mathbf{r}_{k+1} = \mathbf{r}_k + \frac{1}{\gamma}\mathbf{F}(\mathbf{r}_k,t_k) + \sqrt{\frac{2k_BT\,\Delta t}{\gamma}}\mathbf{W}_k. \tag{6}$$

Here, each component of $\mathbf{W}_k$ is a Gaussian random variable with zero mean and unit variance, and $\Delta t = t_{k+1} - t_k$ is the time step.

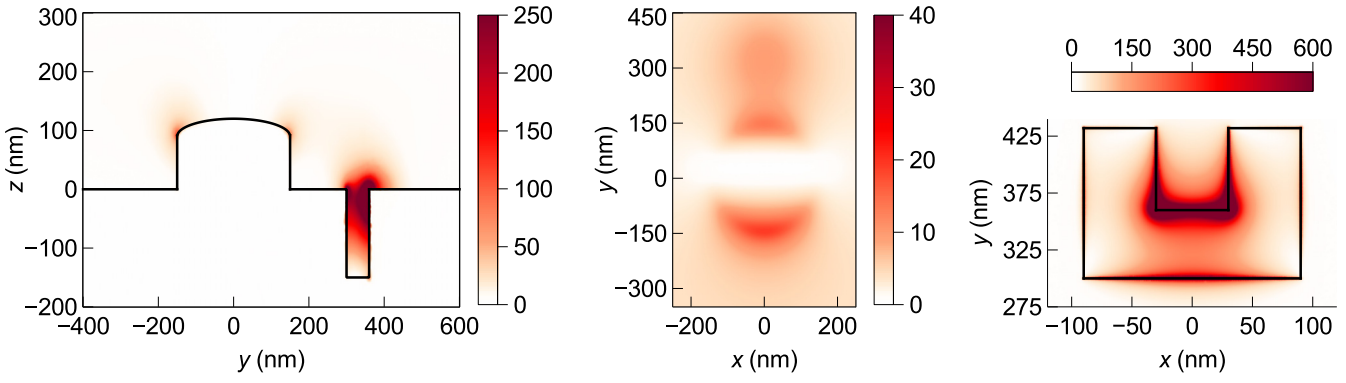

(a) (b) (c)

FIG. 6. Optical field-intensity enhancement, $|\mathbf{E}|^2/|\mathbf{E}_0|^2$ at 1064-nm incident light polarized along the y direction (with no particle in the system). (a) yz cross-section at $x = 0$. (b) xy cross-section at $z = h_{\text{np}}$. (c) xy cross-section at $z = 0$.

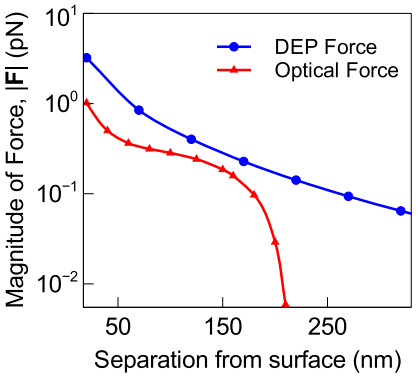

FIG. 8. Comparison of the DEP force and optical force range (y axis in log scale), with $I_{\text{inc}} = 1\,\text{mW}/\mu\text{m}^2$ and $|\mathbf{E_0}| = 0.18\,\text{V}/\mu\text{m}$.

The viscous drag coefficient, γ, depends on the radius of the nanoparticle, viscosity of the medium, and distance of the nanoparticle from the solid surfaces. Taking into account the hydrodynamic interactions with a solid surface, the viscous drag coefficient is given by [39,40]

$$\gamma_{x,y} = \frac{6\pi\eta r_o}{1 - \frac{9r_o}{16z} + \frac{r_o^2}{8z^2} - \frac{45r_o^4}{256z^4} - \frac{r_o^5}{16z^5}}, \tag{7}$$

$$\gamma_z = \frac{6z^2 + 2r_o z}{6z^2 + 9r_o z + 2r_o^2}, \tag{8}$$

where η is the fluid viscosity, r_o is the radius of the nanoparticle, z is the coordinate of the center of the spherical nanoparticle, and the solid surface is assumed to be parallel to the xy plane at $z = 0$. $\gamma_{x,y}$ is used to calculate the x or y component of the position vector and γ_z is used for calculating the z component of the position vector using Eq. (6).

The collisions between the particle and the geometric structures (bottom surface and the nanopillar) are modeled as reflection operations. Taking into account the reflection from the structures and the hydrodynamic interaction corrected viscous drag coefficients, Eq. (6) can be used to accurately model the nanoparticle motion.

VI. SIMULATION AND RESULTS

Using the Brownian dynamics model presented in Sec. V, a trapping event is simulated by observing the motion of a nanoparticle in the DEP and the optical force-field. The initial position of the nanoparticle at $t = 0$ is set at a random point near the trapping structures (less than 1 μm away from the CSE and/or nanopillar). The position of the particle at time t is noted. If the particle position is less than 100 nm away from the trapping structure, the particle is considered to be successfully trapped. This entire simulation can be repeated multiple times to obtain a distribution of nanoparticle position. To quantify the trapping performance, the probability of a trapping event at time t is defined as:

$$p_{\text{trap}}(t) = \frac{N_{\text{trap}}(t)}{N_T}, \tag{9}$$

where N_T is the total number of simulations performed, and $N_{\text{trap}}(t)$ is the number of times the simulation leads to successful trapping of the nanoparticle at time t. For each simulation, it is assumed that only a single nanoparticle is present in the region of interest. This approximation is valid for modeling cases where particle density is low.

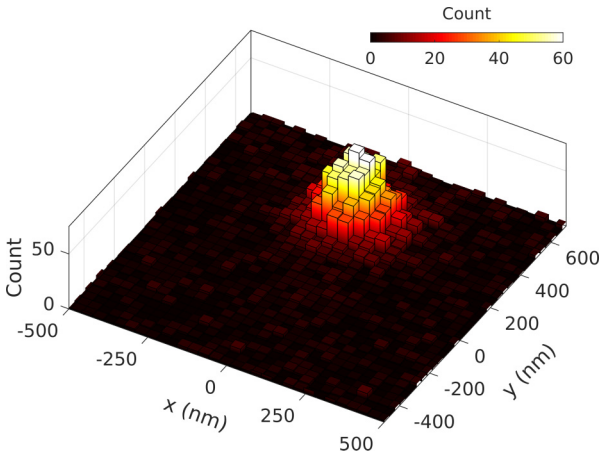

FIG. 9. Nanoparticle position distribution at $t = 0.4$ sec in the xy plane when it is near the CSE top surface ($z \leqslant 250$ nm) for a purely plasmonic trap (no nanopillar).

First, a base case consisting of a purely plasmonic trap is simulated. A CSE without the nanopillar serves as the plasmonic trap. The center of the CSE is considered to be located at (0, 366 nm, 0) to be consistent with later simulations. The nanoparticle motion under the optical force-field is simulated from $t = 0$ to 0.4 s. The optical excitation is kept on throughout this duration. The simulation is repeated $N_T = 35\,000$ times to obtain the position distribution of the nanoparticle. The position distribution in the xy plane is shown in Fig. 9. As particle positions with $z > 250$ nm are far away from the CSE, they are random in nature and are therefore avoided in the figure. It is found that the probability of the nanoparticle being trapped is 5.1% at $t = 0.15$ s and 5.4% at $t = 0.4$ s. The performance of this base structure will be compared against that of the proposed structure.

In the proposed trapping scheme, the DEP force-field is turned on at $t = 0$. It is turned off at $t = 0.15$ s and the optical force-field is turned on. Like the base case, the final time of the simulation is set to $t = 0.4$ s and $N_T = 35\,000$ independent simulations are performed. The particle position distribution near the nanopillar at $t = 0.15$ s is shown in Fig. 10. Particle positions far away from the structure ($z > 370$ nm) are not shown in the plot avoid the addition of unnecessary information. For ease of visualization, the position distribution is divided into two parts: below the nanopillar top surface ($z \leqslant 270$ nm), and above the nanopillar top surface (270 nm $\leqslant z \leqslant$ 370 nm). It can be easily seen from the figures that the nanoparticle positions are clustered around the top and side surfaces of the nanopillar. The probability of the particle being trapped near the nanopillar is 21.56% at $t = 0.15$ s. The higher probability is due to the longer range of the DEP force. It is to be noted that unlike the plasmonic trap, the particle position distribution of the DEP trap is spread over a wider region. However, as the primary objective of the nanopillar is to draw the particles near the CSE, the lack in resolution is not of concern.

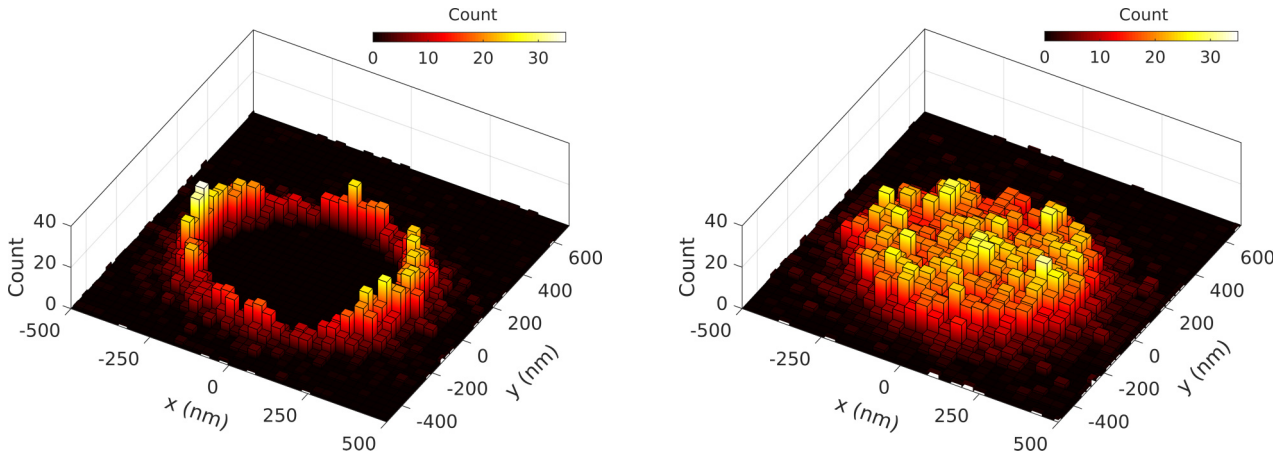

FIG. 10. Nanoparticle position distribution at $t = 0.15$ s in the xy plane when it is near the nanopillar ($z \leqslant 270$ nm and 270 nm $\leqslant z \leqslant$ 370 nm) under the influence of the DEP force-field. (a) Low positions: $z \leqslant h_{\text{np}} + r_o$ (b) High positions: $h_{\text{np}} + r_o \leqslant z \leqslant h_{\text{np}} + r_o + 100$ nm

The DEP trap is turned off and the plasmonic trap is turned on at $t = 0.15$ s. The particle position distribution near the CSE ($z \leqslant 250$ nm) at $t = 0.4$ s is shown in Fig. 11. It can be seen that the position density is very high near the CSE. The second high-density region represents the nanoparticle being trapped near the nanopillar. This is due to the optical response of the nanopillar. The probability of the nanoparticle being trapped near the CSE is found to be 15.45%. The trapping probability near the nanopillar is 2.5%. Since the CSE creates a much stronger optical force-field, the particle is more likely to be trapped near the CSE than near the nanopillar. The trapping probabilities of the base scheme (CSE only) and the proposed scheme (CSE + nanopillar) are listed in Table III. The probability of a successful trap near the CSE is almost three times higher for the proposed scheme. Because the DEP force attracts the nanoparticle near the nanopillar (and thus near the CSE) during time $0 \leqslant t \leqslant 0.15$ s, the probability of the particle being in the trapping range of the CSE is high compared to the base case. As a threefold increase in trapping probability is achieved, it can be concluded that the proposed DEP-assisted plasmonic trap performs significantly better than an isolated plasmonic trap. It should be mentioned that the data of Table III suggests that the nanopillar alone may be good enough as it has the highest trapping event probability. However, the DEP trap from the nanopillar spans a larger volume resulting in poor resolution as can be seen from Fig. 10. The proposed CSE + nanopillar composite scheme has the high resolution of the plasmonic trap which is evident from Fig. 11, and at the same maintains a high trapping event probability.

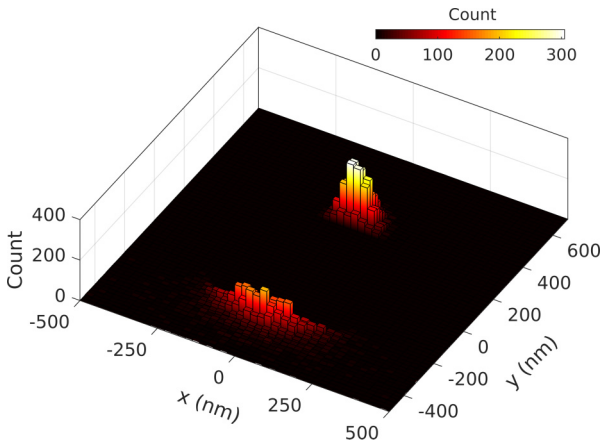

FIG. 11. Nanoparticle position distribution at $t = 0.4$ s in the xy plane when it is near the CSE top surface ($z \leqslant 250$ nm) for the proposed trapping scheme (with nanopillar).

VII. CONCLUSIONS

A DEP-assisted plasmonic trapping scheme is proposed to address the short-trapping-range problem of a conventional plasmonic trap. Numerical simulations show that the long-range DEP force successfully draws particles near the plasmonic trap. As a result, the probability of a successful trapping event is increased by approximately three times. The proposed scheme can be used for single particle (or low particle density) trapping experiments. The scheme can also be used to support large scale parallelization of plasmonic traps for laboratory-on-a-chip applications.

TABLE III. Comparison of trapping performance ($t_1 = 0.15$ s, $t_2 = 0.4$ s).

	Trapping event probability (%)	
Structure	Near nanopillar	Near CSE
CSE only (at $t = t_1$)	—	5.11
CSE only (at $t = t_2$)	—	5.43
CSE + nanopillar (at $t = t_1$)	21.56	0.51
CSE + nanopillar (at $t = t_2$)	2.50	15.45

[1] A. H. Yang, S. D. Moore, B. S. Schmidt, M. Klug, M. Lipson, and D. Erickson, Nature **457**, 71 (2009).

[2] M. D. Wang, H. Yin, R. Landick, J. Gelles, and S. M. Block, Biophys. J. **72**, 1335 (1997).

[3] K. Svoboda and S. M. Block, Annu. Rev. Biophys. Biomol. Struct. **23**, 247 (1994).

[4] A. Ashkin, Phys. Rev. Lett. **24**, 156 (1970).

[5] A. Ashkin, Proc. Natl. Acad. Sci. USA **94**, 4853 (1997).

[6] A. Ashkin and J. M. Dziedzic, Science **235**, 1517 (1987).

[7] M. Righini, P. Ghenuche, S. Cherukulappurath, V. Myroshnychenko, F. J. Garcia de Abajo, and R. Quidant, Nano Lett. **9**, 3387 (2009).

[8] L. Novotny, R. X. Bian, and X. S. Xie, Phys. Rev. Lett. **79**, 645 (1997).

[9] M. L. Juan, M. Righini, and R. Quidant, Nature Photon. **5**, 349 (2011).

[10] P. Hansen, Y. Zheng, J. Ryan, and L. Hesselink, Nano Lett. **14**, 2965 (2014).

[11] Y. Zheng, J. Ryan, P. Hansen, Y.-T. Cheng, T.-J. Lu, and L. Hesselink, Nano Lett. **14**, 2971 (2014).

[12] Y. Zheng, J. Ryan, P. Hansen, Y.-T. Cheng, T.-L. Lu, and L. Hesselink, in *CLEO Science and Innovations* (Optical Society of America, San Jose, CA, 2014), pp. STh4H–6.

[13] M. Righini, A. S. Zelenina, C. Girard, and R. Quidant, Nature Phys. **3**, 477 (2007).

[14] K.-Y. Chen, A.-T. Lee, C.-C. Hung, J.-S. Huang, and Y.-T. Yang, Nano Lett. **13**, 4118 (2013).

[15] V. Yannopapas, Phys. Rev. B **78**, 045412 (2008).

[16] M. L. Juan, R. Gordon, Y. Pang, F. Eftekhari, and R. Quidant, Nature Phys. **5**, 915 (2009).

[17] K. Wang, E. Schonbrun, P. Steinvurzel, and K. B. Crozier, Nature Commun. **2**, 469 (2011).

[18] K. Wang and K. B. Crozier, Chem. Phys. Chem. **13**, 2639 (2012).

[19] J. C. Ndukaife, A. V. Kildishev, A. G. A. Nnanna, V. M. Shalaev, S. T. Wereley, and A. Boltasseva, Nature Nanotechnol. **11**, 53 (2016).

[20] B. J. Roxworthy, K. D. Ko, A. Kumar, K. H. Fung, E. K. Chow, G. L. Liu, N. X. Fang, and K. C. Toussaint Jr, Nano Lett. **12**, 796 (2012).

[21] N. G. Green and H. Morgan, J. Phys. Chem. B **103**, 41 (1999).

[22] N. G. Green and H. Morgan, J. Phys. D **30**, L41 (1997).

[23] P. R. Gascoyne and J. Vykoukal, Electrophoresis **23**, 1973 (2002).

[24] T. Yamamoto and T. Fujii, Nanotechnology **18**, 495503 (2007).

[25] X. Shi and L. Hesselink, JOSA B **21**, 1305 (2004).

[26] J. Matteo, D. Fromm, Y. Yuen, P. Schuck, W. Moerner, and L. Hesselink, Appl. Phys. Lett. **85**, 648 (2004).

[27] J. Pappo, T. H. Ermak, and H. J. Steger, Immunology **73**, 277 (1991).

[28] M. Ozkan, M. Wang, C. Ozkan, R. Flynn, and S. Esener, Biomed. Microdevices **5**, 61 (2003).

[29] J. Voldman, R. A. Braff, M. Toner, M. L. Gray, and M. A. Schmidt, Biophys. J. **80**, 531 (2001).

[30] R. Pethig, Biomicrofluidics **4**, 022811 (2010).

[31] C. Rosales and K. M. Lim, Electrophoresis **26**, 2057 (2005).

[32] X. Wang, X.-B. Wang, and P. R. Gascoyne, J. Electrostat. **39**, 277 (1997).

[33] M. A. Ordal, L. L. Long, R. J. Bell, S. E. Bell, R. R. Bell, R. W. Alexander, and C. A. Ward, Appl. Opt. **22**, 1099 (1983).

[34] P. B. Johnson and R.-W. Christy, Phys. Rev. B **6**, 4370 (1972).

[35] F. Hao, C. L. Nehl, J. H. Hafner, and P. Nordlander, Nano Lett. **7**, 729 (2007).

[36] G. Volpe and G. Volpe, Am. J. Phys. **81**, 224 (2013).

[37] T. Schnelle, T. Müller, G. Gradl, S. G. Shirley, and G. Fuhr, Electrophoresis **21**, 66 (2000).

[38] D. J. Higham, SIAM Rev. **43**, 525 (2001).

[39] E. Schäffer, S. F. Nørrelykke, and J. Howard, Langmuir **23**, 3654 (2007).

[40] A. Banerjee and K. D. Kihm, Phys. Rev. E **72**, 042101 (2005).